Design, Manufacture, and Experimental Validation of a Hydraulic Semi-Active Knee Prosthesis

Zhennan Li, Yang Han, Chunbao Liu, Haohua Xiu, Guowu Wei, *Member, IEEE*, and Lei Ren, *Member, IEEE*

***Abstract*— In this article, a new hydraulic semi-active knee (HSAK) prosthesis is proposed. Compared with knee prostheses driven by hydraulic-mechanical coupling or electromechanical systems, we novelly combine independent active and passive hydraulic subsystems to solve the incompatibility between low passive friction and high transmission ratio of current semi-active knees. The HSAK not only has the low friction to follow the intentions of users, but also performs adequate torque output. Moreover, the rotary damping valve is meticulously designed to effectively control motion damping. The experimental results demonstrate the HSAK combines the advantages of both passive and active prostheses, including the flexibility of passive prostheses, as well as the stability and the sufficient active torque of active prostheses. The maximum flexion angle in level walking is about 60°, and the peak output torque in stair ascent is greater than 60Nm. Relative to the daily use of prosthetics, the HSAK improves gait symmetry on the affected side and contributes to the amputees better maintain daily activities.**

***Index Terms*— Knee prosthesis, hydraulic, semi-active drive, low passive friction, high transmission ratio.**

I. Introduction

TRANSFEMORAL amputees confront many inconveniences in daily life due to the absence of lower limbs. The vast majority of amputees utilize fixed or variable damping prostheses, collectively known as passive knees (PKs) [1], [2]. The PKs can support the amputees during the stance phase and are compliantly followed by the residual thigh to provide free passive flexion and extension during swing. The microprocessor-controlled knees (MPKs) present better performance by adjusting the damping force of the actuator [3]. Nonetheless, the PKs lack the active power, resulting in the inadequate robustness in the swing phase, and lead to insufficient extension in some cases, which jeopardizes the stability of the prosthesis in subsequent contact and may cause the amputees to stumble. In addition, the intact limbs have to compensate more for the absent joint functions, which lead to lower-back pain [4] and more physical consumption than healthy people [5].

In order to resolve the above problems, more recent attention has focused on the research of the active knees (AKs). The AKs can upgrade comfort and range of motion, and various studies have demonstrated the advantages [6]. UT Dallas prosthesis was driven by a high-power motor connected with the timing belt and the ball screw [7], [8]. And Goldfarb et al. [9], [10], [11] used a brushless dc motor and a three-stage belt transmission to drive the joint. These active electric prostheses drive the knee joint directly with a typical speed reduction transmission greater than 100:1 and cause more rigid joints. The AKs force the knee swing actively rather than swings freely, which results in more drastic discomfort on the residual limb after long-term use [12]. Thus, the Power Knee and the OSL diminished the stiffness and inertia of the drive system by series elastic actuator (SEA) [13], [14]. As a matter of fact, the motor of AKs needs to generate a substantial torque to support the knee joint in the stance phase, which consumes unnecessary electricity [15]. Hence, the research on semi-active knees (SAKs) with passive components is progressively emerging [16], [17]. The MIT knee was driven by a clutchable series-elastic actuator (CSEA) [18]. In the stance phase, the clutch is turned on and the stiff springs support the amputees. While in the swing phase, the clutch is off and the joint is actively driven by the SEA. Lenzi et al. [19], [20], [21] designed an actively variable transmission (AVT) in the Utah knee to switch the passive and active modes. The prosthesis supports level walking with low passive transmission ratio and stairs movement with a high active ratio. However, the ratio switching takes a while.

Manuscript received 15 September 2022; revised 3 January 2023; accepted 14 February 2023. Date of publication 16 February 2023; date of current version 24 February 2023. This work was supported in part by the National Key Research and Development Program of China under Grant 2018YFC2001300; in part by the Young and Middle-Aged Scientific and Technological Innovation and Entrepreneurship Outstanding Talents (Team) Project (Innovation) of Jilin Province under Grant 20210509007RQ; and in part by the Fundamental Research Funds for the Central Universities, Jilin University, under Grant 2020-JCXK-16. *(Corresponding authors: Chunbao Liu; Lei Ren.)*

This work involved human subjects or animals in its research. Approval of all ethical and experimental procedures and protocols was granted by the Second Hospital of Jilin University under Application No. 2021072.

Zhennan Li, Yang Han, and Chunbao Liu are with the Key Laboratory of Bionic Engineering, Ministry of Education, School of Mechanical and Aerospace Engineering, Jilin University, Changchun 130022, China (e-mail: lizn20@mails.jlu.edu.cn; hanyang19@mails.jlu.edu.cn; liuchunbao@jlu.edu.cn).

Haohua Xiu and Lei Ren are with the Key Laboratory of Bionic Engineering, Ministry of Education, Jilin University, Changchun 130022, China, and also with the School of Mechanical, Aerospace and Civil Engineering, University of Manchester, M13 9PL Manchester, U.K. (e-mail: xiuhh@jlu.edu.cn; lei.ren@manchester.ac.uk).

Guowu Wei is with the School of Science, Engineering and Environment, University of Salford, M5 4WT Manchester, U.K. (e-mail: g.wei@salford.ac.uk).

This article has supplementary downloadable material available at https://doi.org/10.1109/TNSRE.2023.3246071, provided by the authors.

Digital Object Identifier 10.1109/TNSRE.2023.3246071

In fact, the most current electric prostheses are faced with the problems of high impedance, large transmission ratio [12]. During the swing, these prostheses are always actively driven, rather than following the thigh like PKs. It has been shown that a low impedance actuator allows the knee to swing passively and follow the stump motion harmoniously. The AKs or SAKs gain low impedance by decreasing high friction devices or reducing the transmission ratio. However, the low transmission ratio also leads to a low active torque, otherwise, the knee will be heavy if a large torque motor is chosen. Gregg et al. [22] designed a low impedance actuator through a custom planetary gear mechanism and applied it to the power leg. The leg provides passive knee swing motion, decreasing the power requirement for swing flexion, but its large weight limits clinical acceptance. The SCSA knee [23], [24], [25] is actively driven by a one-stage gear reduction and ball screws embedded inside the piston rod. On the RTFP knee [26], the motor output shaft is directly connected to the knee joint through the timing belt to assist the knee motion. The SCSA knee and the RTFP knee merged hydraulic damping regulation in parallel with motor active drive to achieve a low active ratio and backdrivability. The SCSA knee and the RTFP knee both allowed the prosthesis to swing freely. But the friction of the drive systems is higher than that of the passive hydraulic prosthesis as the active drive system and hydraulic damping system are not separated during the movement. In addition, the low transmission ratio limits the active extension torque (7.5-8.5Nm) compared to other powered prostheses in stair ascent.

The prosthesis described here is designed to retain the desirable characteristics of both semi-active and active knees. In level walking, the prosthesis must have low power consumption in the stance phase, free flexion and active extension in the swing phase. In complex environments such as stair ascent, the prosthesis must be able to provide sufficient torque. In addition, the battery should satisfy at least one day of walking for the average user (2300±1500 steps) on a single charge [24]. Therefore, the most important problem to be solved is how to make the prosthesis compatible with both free swing and adequate torque output.

The advantage of hydraulic transmission is that it can be easily converted rotary motion into linear motion [27], [28]. It was confirmed that hydraulic system can perform better in friction than gears [29]. The major contributions of our design are as follows:

1) In this article, an improved prosthesis called Hydraulic Semi-Active Knee (HSAK) was reported to enhance the function of SAKs. The proposed prosthesis solves the problem existing in the current semi-active prostheses, which is incompatibility between low passive friction and high active transmission ratio. The novel prosthesis integrated of two independent active and passive drive subsystems. The principle, design and manufacture of the prosthesis was clarified.
2) The HSAK has both the characteristics of the harmony of adjustable damping prostheses and the versatility of active prostheses. In contrast to the advanced knees [24] and [26], where the low-ratio was used to minimize friction but result in low-torque transmission, the proposed prosthesis allows lower passive friction and more sufficient active torque.

II. Design and Manufacture

This section presents the design and manufacture of the HSAK. The hydraulic principal is described, followed by the details for a critical component, i.e., the rotary damping valve, the integrated block, and the control system.

A. Hydraulic Principle

The semi-active integration actuator of the HSAK was a closed-circuit hydraulic system. As can be seen from Figs.1(a) and (b), the drive system was designed and consisted of three sections: the active section (including active motor, hydraulic pump), the damping section (consisting of rotary damping valve, damping motor), and the actuator section (containing spring, accumulator piston, piston and rod). The actuator section is connected with the damping and active sections to form the damping adjustment and active driving subsystems, respectively. The three sections are incorporated together by a hydraulic block. In Fig.1, the block connects ports A, C, and E together, and ports B, D, and F together.

The working principles of the hydraulic system are illustrated in Figs.1(a) and (b). In early stance phase, the pump does not work and the prosthesis locks the knee by the closed valve. During passive flexion, the piston is subjected to downward pressure, and the oil through the rotary valve from the port F reaches the port E. The damping force is regulated via the flow area of the rotary valve. While the oil flows reversely in passive extension. When the joint is actively extended, the valve is closed and the oil pressurized by the pump is transported from port E to port F to drive the rod upward. The reversal oil moves the rod downward. The energy storage system involves a spring accumulator to reserve the oil volume difference generated by piston motion during knee flexion and releases it during extension.

The HSAK employs a semi-active mode (SAM) in level walking. During the SAM, the flexion motion is adjusted by the valve, and the extension motion is actively driven by the pump. In extension period, the oil in the energy storage system increases the pressure of port A to ensure the pump is fully supplied with oil. In the event of a power failure, the energy storage system provides the passive extension torque as an aid. In addition, the HSAK can assist amputees in step-over stair ascent via active swing motion and active stance extension.

In summary, the HSAK is equipped with an energy recovery device and integrates active and damping subsystems. When the damping subsystem is engaged, the HSAK supplies the benefits of an MPK, meanwhile, it also purveys powerful assistance when the active subsystem is engaged for special tasks (e.g., the late swing phase of walking and the active phase of step-over stair ascent). In particular, in the SAM, the HSAK due to the low friction has a passive flexion function in swing phase in walking like MPKs, which is a unique

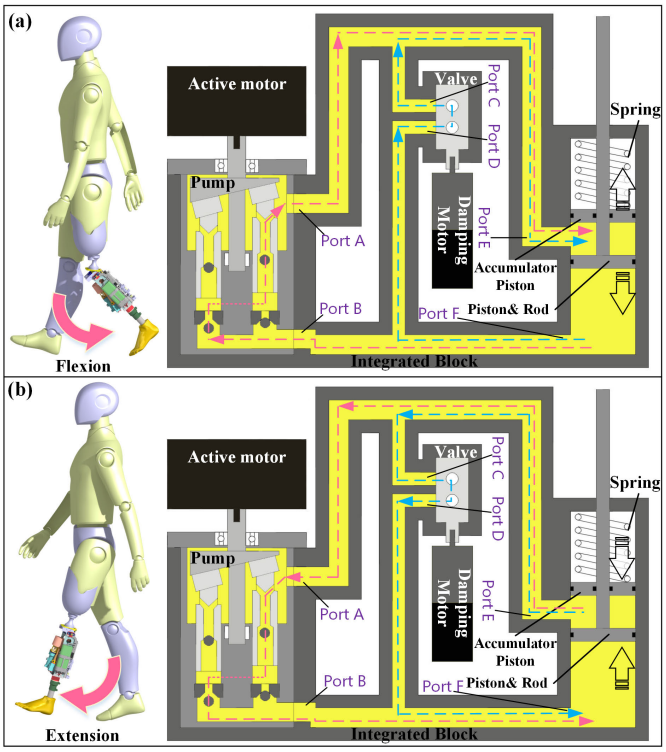

Fig. 1. Hydraulic driving principle of (a) knee flexion and (b) knee extension by HSAK (blue and red arrows indicate the directions of the hydraulic oil flow in the passive and active modes, respectively).

benefit of the hydraulic knee compared to the electric power knee. Moreover, the damping and active subsystems can work together to guarantee two subsystems switch smoothly.

B. Rotary Damping Valve

The control of motion damping is a key issue in knee prostheses. To solve this, a rotary damping valve is developed in this paper, the valve has a simple structure but favorable dynamic properties. It can be seen from Fig.2(a) that the rotary valve mainly comprises a valve sleeve, valve spool, and stop block. The valve spool has a radius of 7.5mm, and the inlet and outlet ports are connected by an oil flute with a surface depth of 5mm. Three pressure-equalizing grooves are evenly designed on both sides of the flute to balance the radial forces generated during work [30]. Sealing components are used to separate the inlet port, the outlet port and the external environment. A clearance seal is placed between the spool and valve sleeve. All components are installed inside a hole in the integrated block.

The damping valve structure has the merits of continuous linear variation of flow area. In the valve, both the groove width and the oil ports diameter are 3mm, thus the maximum flow area is calculated about 7mm^2. The red curve cutting the blue circle in Fig.2(b) presents the transformation of the spatial rotation to planar translation. The valve flow area can be divided into two parts for calculation: S_{up} and S_{down}. It is assumed that there is no relative motion between the valve sleeve and integrated block and that the plane expanded by the valve port is approximately circular, then the relationship

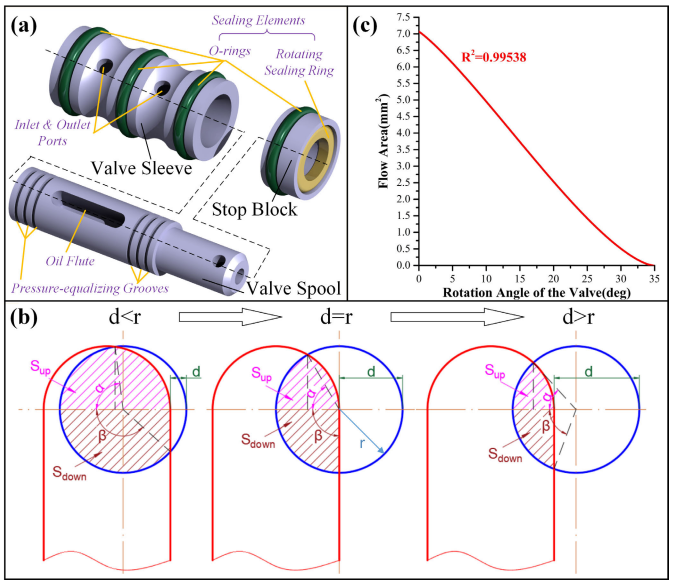

Fig. 2. (a) Three-dimensional structure of the rotary valve: valve sleeve, valve spool, stop block. (b) Change in flow area during rotation of the valve spool and the (c) calculated linearity.

between the rotation angle θ_{valve} and valve flow area S could be obtained through (1)-(6), and the result is shown in Fig.2(c).

$$S = S_{up} + S_{down} \tag{1}$$

$$S_{up} = (\frac{1}{2}r^2 \times \alpha - \frac{1}{2}r \times \frac{d}{2}sin\alpha) \times 2 \tag{2}$$

$$S_{down} = \frac{1}{2}r^2 \times \beta + \frac{1}{2}r \times (r-d)sin\beta \tag{3}$$

$$\alpha = cos^{-1}\frac{d}{2r} \tag{4}$$

$$\beta = \pi - cos\frac{r-d}{r} \tag{5}$$

$$d = R_{sleeve} \times \theta_{valve} \tag{6}$$

where r is the oil hole radius of the valve inlet and outlet, d is the relative displacement between the spool and the sleeve, R_{sleeve} is the radius of the valve sleeve. The linearity R^2 was 0.99538, which which ensured proportional relationship between flow area and the angular displacement to control the valve better [31].

The ANSYS/Fluent software, one of the most practical simulation softwares for CFD, is used to evaluate and analyze the internal flow field of the spool. Based on the biomechanical regulation of healthy knee joint movement [32], the maximum force on piston was assumed about 1500N, and the maximum hydraulic pressure was about 5MPa during the level walking of a 100kg user. Thus, the boundary condition of inlet pressure and outlet pressure were set to 5MPa and 0MPa, respectively. In addition, the density, dynamic viscosity, and temperature of hydraulic oil were 880kg/m^3, 0.0258Pa·s, and 293K, respectively. It was assumed that there was no heat exchange between the wall of the basin, the fluid, and the external environment. The gravitational potential energy and gap between the spool and sleeve were also omitted. The internal flow pattern of the basin was considered to be turbulent, so the standard turbulence model was chosen for simulations. Further details

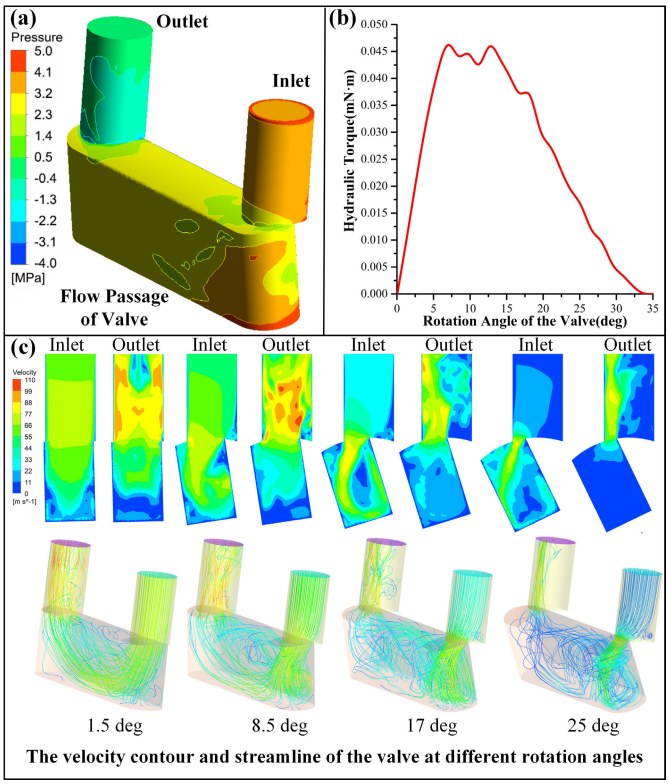

Fig. 3. (a) Pressure contour when the valve spool rotates 8.5°. (b) Simulation curve of the change in the steady flow torque during the rotation of the valve spool. (c) Streamline diagrams and velocity nephograms of the inlet and outlet flow fields for different rotation angles of the valve spool.

of the grid model, turbulence model, boundary conditions, and solution strategy are presented in the Supplementary Materials.

The rotary valve fluid domain comprises three parts: the inlet, the outlet, and the flow passage of valve channel. In addition, the pressure contour at a rotation angle of 8.5° is shown in Fig.3(a). The inlet pressure was 5MPa, and the outlet pressure was 1.4MPa; which indicates that the pressure decreased when hydraulic oil flowed through the valve and that the valve had an obvious damping effect. In the damping valve, the steady flow torque is a critical issue that affects the rotary valve characteristics. The steady flow torque is in the opposite direction of the fluid momentum change in the circumferential direction, and it is an important part of the movement resistance of the valve [33].

Looking at Fig.3(b), the results of steady flow torque data at different rotation angles of the spool at a pressure of 5MPa were extracted by Ansys-Fluent. It is apparent that the maximum steady flow torque was 46.2mNm for rotation angles of 7°–13°, which was far less than the 170mNm rated torque of valve motor (ECXSP13M with GPX16 83:1 and ENX13 1024IMP, Maxon). Fig.3(c) presents the streamline diagram and velocity nephogram of the inlet and outlet flow fields of the rotary valve at different rotation angles. It can be seen that with the change of spool rotation angle, fluid flow direction and velocity vector in the valve are varying. For a small rotation angle (1.5°), the velocity distributions of the inlet and outlet were relatively uniform, and the hydraulic oil flowed from the bottom of the inlet through the outlet, and the streamline distribution was much concentrated. When the rotation angle mounting to 8.5°, the velocity nephogram displays that the high-speed hydraulic oil impacted the side and bottom surfaces and reflected at the spool inlet. At the outlet of the valve spool, the flow velocity of the hydraulic oil decreased slightly with a radial ejection. In the streamline diagram, the fluid at the inlet was divided into two parts inside the rotary valve. The small part of the oil flowed through the outlet after impacting the bottom of the valve channel while the most impacted the side again and spiraled. Finally, the two parts of the oil gathered at the outlet. As the rotation angle went up to 17°, the inlet oil velocity enhanced, and the impact on the wall was more obvious. And the oil moved almost entirely in a spiral shape, and the outlet velocity decreased relative to that at the 8.5°. Further increasing the rotation angle to 25° resulted in the oil motion similar to that at 17°, but the average outlet velocity became neap. Enlarging the rotation angle gradually decreased the opening of the valve port, strengthened the damping effect of the rotary valve, and reduced the outlet flow rate and pressure. The numerical simulations clarified the transmission process of the internal oil motion while the damping valve was operating. These graphics and results cannot be obtained through experiments and have not been reported in other prostheses research.

C. System Integration

To reduce the overall size and weight, we designed a hydraulic integrated block which has many holes to form inside channels to connect each sectionin the drive system as shown in Fig.4(a). The process holes are sealed with plugs (QD060E) and screws. The drive system is attached to the prosthesis by bearings in the rod and cylinder end cover.

The internal channels with a diameter of 5mm of the integrated block are depicted in Fig.4(b) and Fig.4(c). From Fig.1 and Fig.4, the oil circuit of the block connects the pump port 1 (port A), the valve port 1 (port C), and the cylinder port 2 (port E) together, and the pump port 2 (port B), the valve port 2 (port D), and the cylinder port 2 (port F) together.

During passive flexion, as shown in Fig.4(b), the oil moves from cylinder port 2 into the other side of the cylinder piston through valve port 2, valve port 1, and cylinder port 1, as the blue channels and the white arrows shown. Correspondingly, the oil transports in reverse in passive extension. Due to the volumetric efficiency, some of the oil will inevitably leaks when the pump rotates, and this part of the oil needs to be discharged outside the pump through the drainage port. The green dotted line displays the direction of the leakage. And the leakage increases with the pressure. During active extension, as shown in Fig.4(c), the active subsystem is engaged but the damping subsystem is not, which means that the valve is closed and no oil flows in the valve as the black channels shown. The oil in the cylinder enters pump port 1 from the cylinder port 1, and the high-pressure oil from pump port 2 enters the cylinder through cylinder port 2 to extend actively, as the red channels and the red arrows shown. At this time, the leaked oil in the high-pressure state ingresses into the pump again through pump port 1, which does not affect the system.

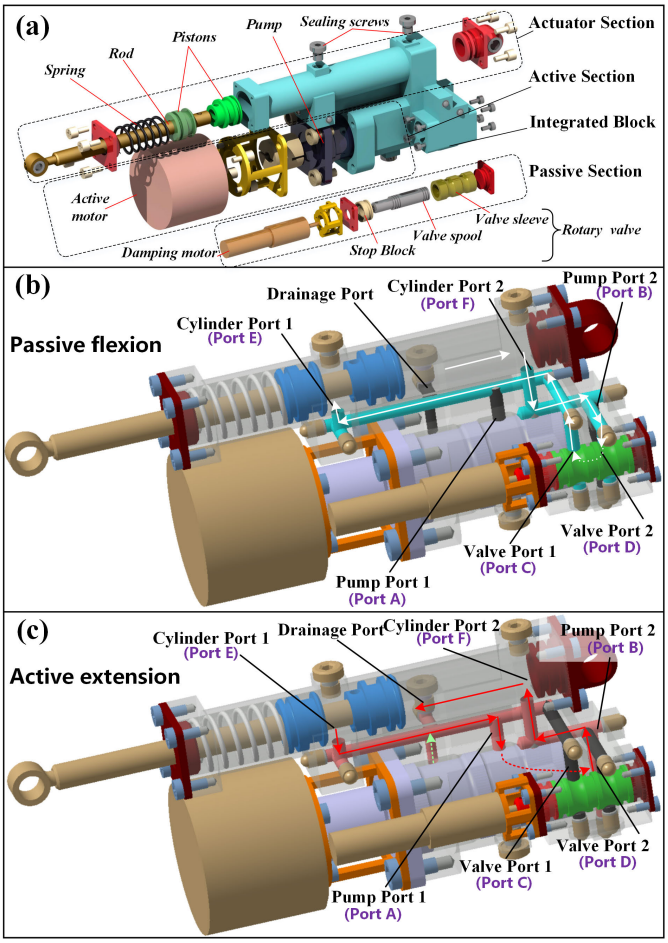

Fig. 4. (a) Assembly of the HSAK drive system. Drive system operating principle when passive flexion (b) and (c) active extension: The black channels indicate that the oil is stationary, and the arrows indicate the direction of oil flow.

During active flexion in the swing phase of stairs ascent, the pump reverses and the direction of the oil is opposite except the leakage. The oil flows from the pump port 1 to the cylinder port 1 and prevents the oil flowing from the drainage port. The pressure at drainage port is equal to the active drive pressure of the system. In the swing phase, the oil pressure of the system is relatively low, so the drainage chamber does not fail.

The diameter of pistons and rods are 22mm and 10mm, respectively. The stiffness coefficient of the spring is 7.5N/mm, and was about 10mm pre-compressed during installation to balance the piston friction and increase passive extension torque. Figs.5(a) and (b) exhibit the overall drive system and the fully assembled knee, respectively. The connecting platform was linked to the socket by a nut. A uniaxial load cell was fixed to measure the force of the shank. A high-precision digital potentiometer (GT-D WXXY) was used to get the angle of the knee joint. An inertial measurement unit (IMU 6050) was mounted on the embedded board. The 2800mAh capacity battery comprising six Samsung cores (INR18650-30Q) was applied to meet the user's exercise needs for at least a whole day.

From Fig.5(c) we can see the mechanism of the HSAK simplified into two triangles, while Points P, O, and R represent

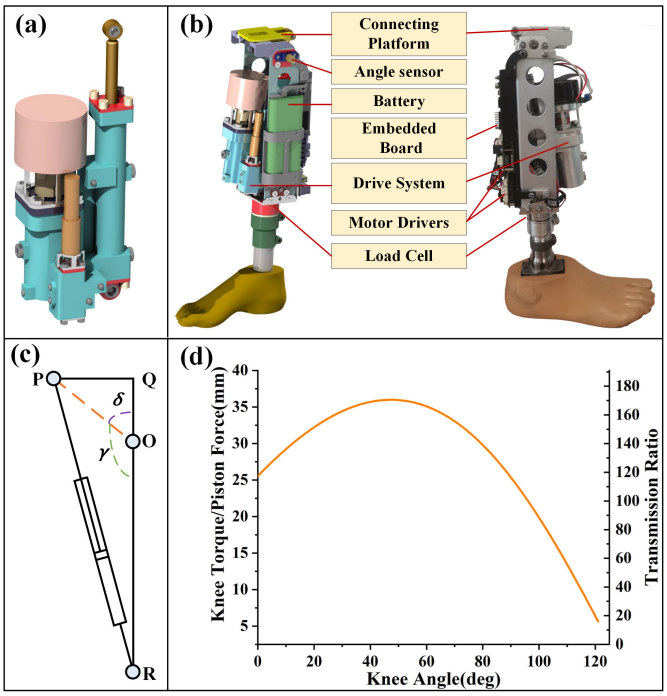

Fig. 5. (a) Overall HSAK drive system. (b) HSAK system integration and prototype. (c) Mechanism. (d) Functional relationship between the knee angle and transmission ratio of the piston force and knee torque.

three rotating pairs, respectively. The functional relationship between the knee angle θ_{knee} and,arm length L_A of piston force F_p and, and the transmission ratio n can be obtained by follows.

$$\delta = arctan\frac{l_{PQ}}{l_{QO}} \tag{7}$$

$$l_{OP} = \sqrt{{l_{PQ}}^2 + {l_{QO}}^2} \tag{8}$$

$$\gamma = 180^\circ - \delta - \theta_{knee} \tag{9}$$

$$l_{RP} = \sqrt{{l_{OP}}^2 + {l_{OR}}^2 - 2 \times l_{OP} \times l_{OR} \times cos\alpha} \tag{10}$$

$$L_A = \frac{T_k}{F_p} = l_{OR} \times \frac{sin\alpha}{l_{RP}} \times l_{OP} \tag{11}$$

$$n = \frac{T_k}{\tau_m} = \frac{2\pi \times S \times L_A}{V_P} \tag{12}$$

where l_{PQ}, l_{QO}, l_{OP}, l_{PQP}, l_{RP}, l_{OR} are the length of links PQ, QO, OP, PQ, RP, OR respectively; T_k is the theoretical knee torque; τ_m is the motor torque; S is the effective area of the piston; V_P is the displacement of the pump.

Fig.5(d) exposes the arm length and the transmission ratio of active extension curve. When the knee angle is 60°, the arm length is 35mm. A 150W brushless motor (Maxon EC flat 60 150W, nominal torque is 401mNm) is used for the power requirements in stair ascent. The 0.5mL/r displacement pump (MP050-A, Chongqing, China) furnishes the active drive for the actuator. The transmission ratio between the knee joint and the motor is 126:1-174:1 based on typical knee angle range from 0° to 90°. The motor would support the knee with a nominal torque of about 50-69Nm. Assuming a total transmission efficiency η of 75%, the motor would still assist the knee with an active torque of 38-52Nm. In summary, the

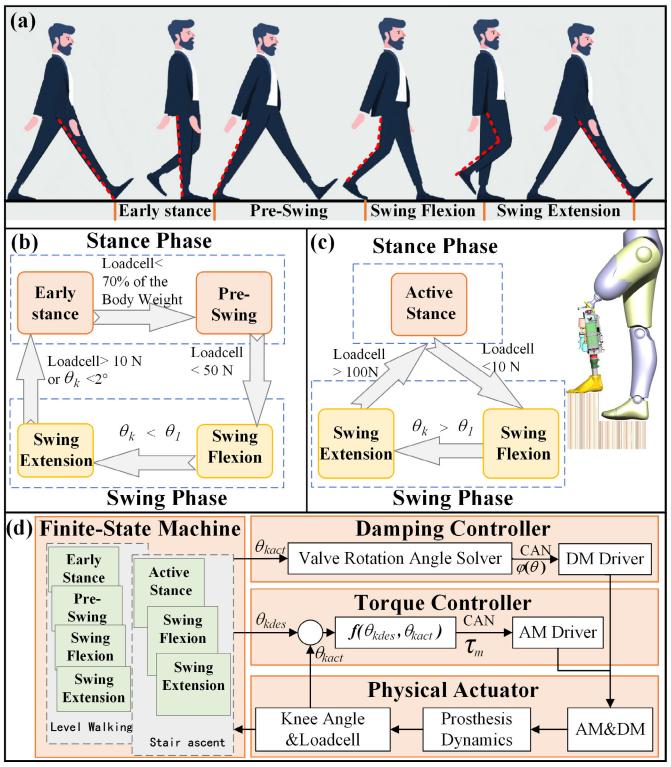

Fig. 6. (a) Division of the gait cycle into phases during level walking. (b) Finite-state machine (FSM) for level walking. (c) FSM for stair ascent. (d) Block diagram of the control system showing the processing stages: FSM, controllers, and physical actuator output.

HSAK has a range of motion of 0° −120°, overall height of 258mm, and total weight of 2.68kg (including the 300g battery).

D. Control System

A finite-state controller was designed for the HSAK. Referring to Fig.6(a)-(c), the level walking can be divided into four phases: Early Stance (ES), Pre-Swing (PS), Swing Flexion (SF), and Swing Extension (SE), and the step-over stair ascent can be divided into three phases: Active Stance (AS), Swing Flexion (SF), and Swing Extension (SE). In all modes, the rotary valve is completely closed and the pump is stationary in the initial state.

The finite-state controller for level walking is set out in Fig.6(b). To guarantee user safety, the HSAK neglects the flexion and extension of the joint in the stance phase of level walking (by following the protocol of the other advanced prostheses [20], [22], [24]). The damping motor (DM) and active motor (AM) are not working neither in the ES phase, and the knee is locked by the closed valve. When the load cell is less than 70% of the body weight, the prosthesis enters the PS phase. In this phase, the DM is engaged and gradually opens the rotary valve to promote passive flexion. Based on the PID parameters tuned by the motor driver (EPOS4 50/1.5, Maxon), the maximum dynamic and static errors of the valve motor are 0.6 degrees and 0.3 degrees respectively. Then, the load cell value is less than 50N. In the SF phase, the DM is engaged to keep flexion damping at a low level, and the knee flexes passively to the maximum flexion angle θ_1. At the SE phase, the DM is driven to quickly close the rotary valve while the AM actively extends. The knee extends to 2°, and the knee angle and load cell value are used as criteria to judge the state at the end of the swing phase. Fig.6(c) illustrates the control of the HSAK for step-over stair ascent. If the load cell value is less than 10N, the prosthetic side enters the SF phase. The knee joint is actively flexed to the θ_1. After that, the prosthesis is actively extended to the preset position θ_2. Then the amputee puts the artificial foot on the next stair. When the force is greater than 100N, the HSAK enters the AS phase. The AM drives the pump for active extension to assist the user with ascending the stairs.

The HSAK is controlled via a custom-built embedded system which was programmed by using C and incorporated with an IMU, an SD card, a Bluetooth, and a microcontroller (STM32F429IGT6). The motor torque drives communicate with the microcontroller via CAN bus. The block diagram of the control system with three stages can be seen in Fig.6(d): the finite-state machine, the damping and torque controllers and the actuator output. The motion mode is switched manually by Bluetooth.

In the PS and SF phase of level walking, the passive damping controller works, the angle of the valve $\varphi(\theta)$ is computed as shown in (13).

$$\varphi(\theta) = \theta_{kact} k(\theta) + c \tag{13}$$

where θ_{kact} is the actual angle of the knee. The control parameters $k(\theta)$, and c are tuned according to the subject test.

In the SE phase of level walking and in the SF and SE phase of step-over stair ascent, the active torque controller works to assist the joint rotation. The torque of the active motor τ_m and knee joint are calculated as shown in (14)-(15).

$$\tau_m = k_p(\theta_{kdes} - \theta_{kact}) + k_d(\theta'_{kdes} - \theta'_{kact}) \tag{14}$$

$$T_{ka} = n\tau_m\eta \tag{15}$$

where θ_{kdes}, k_p and k_d are the target angle of the knee, the proportional gain and the derivative gain, respectively; T_{ka} is the actual torque output to the knee joint by the drive system. The control parameters of different phases are adjusted according to experiments.

In the AS phase of step-over stair ascent, the knee torque of the healthy increases from zero to a maximum and declines to zero for a fully extended knee joint position [19], [34]. Accordingly, in the HSAK, the τ_m changes with the knee angle, as shown in (16).

$$\tau_m = \frac{\theta_{kact} - \theta_3}{\theta_{Tmax} - \theta_3}\tau_{max} \tag{16}$$

where τ_{max} and θ_{Tmax} are the maximum motor torque and the corresponding knee angle during the AS phase, respectively. Moreover, when $\theta_{kact} > \theta_{Tmax}$, $\theta_3 = \theta_2$, when $\theta_{kact} < \theta_{Tmax}$, $\theta_3 = 0$.

III. Bench-Top Experiments

In order to assess the friction of the system and the effect of the hydraulic energy storage principle in Fig.1, the bench-top

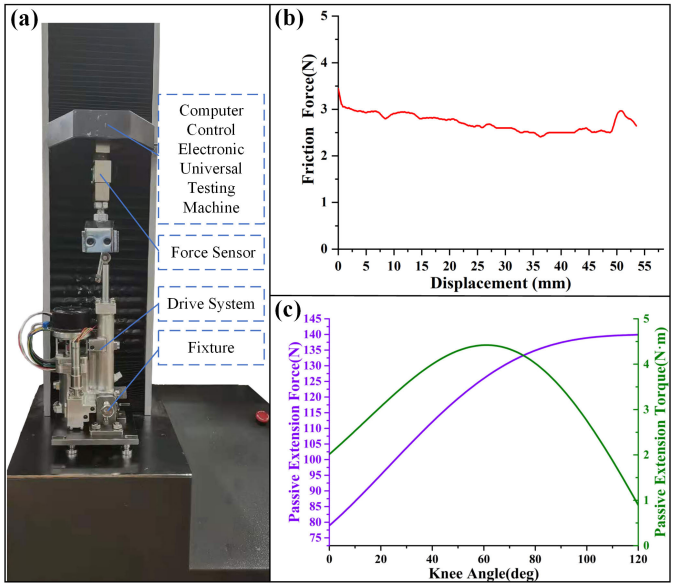

Fig. 7. (a) Experimental bench of the energy storage system. (b) Curve of the relationship between the friction force and piston displacement. (c) Curve of the relationship between the passive extension torque and knee angle.

experiments were carried out. In Fig.7(a), the driving system was fixed onto an electronic universal experiment machine. The valve opening was adjusted to the maximum. The machine stretched or compressed the hydraulic cylinder and recorded the force and displacement.

In the friction force test, the spring was removed and the speed of the rod was 1cm/s. The results of the rod force are demonstrated in Fig.7(b). Due to the machining tolerances, the friction force fluctuates during the piston movement. The average friction is about 3N, which is smaller than 6N in [24] and 200N in [26]. It shows that independent hydraulic transmission provides a lower passive motion resistance than coupling hydraulic and mechanical. The low friction ensures passive flexion and extension performance of the prosthesis in the damping subsystem. In the test of the energy storage system, the piston rod was compressed to the bottom, then the machine was upward fed and the extension force was measured. The functions relating the knee angle to the passive extension force and the passive extension torque are obtained through (7)-(11), as shown by the purple and green curves, respectively, in Fig.7(c). The maximum passive extension torque is 4.42Nm at a knee flexion angle of 60°. The result is over 8 times more than that in [24] and is more helpful as a passive aid to assist extension in a power failure.

IV. Human Subject Experiments

The HSAK was tested to highlight its kinematic and kinetic abilities in clinical experiments and provide biomechanical data for future researchers (Supplementary Video). Two male unilateral femoral amputees with nonvascular were invited to participate in the experiments (Subject 1:31years, 60kg, 1.69m; Subject 2:38years, 80kg, 1.74m).In Fig.8 and Fig.9, the subjects were invited to test the HSAK in level walking and step-over stair ascent with a self-selected suitable speed.

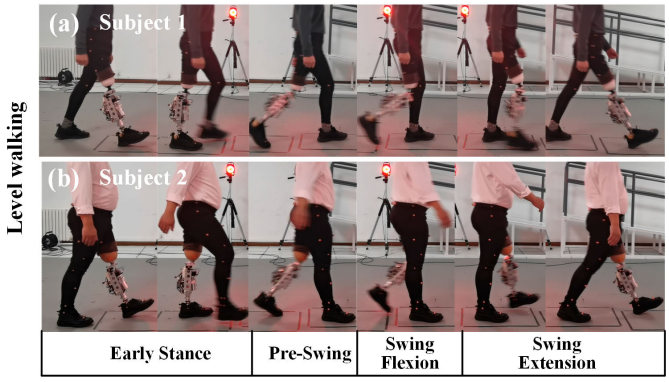

Fig. 8. The subjects wear the HSAK in level walking.

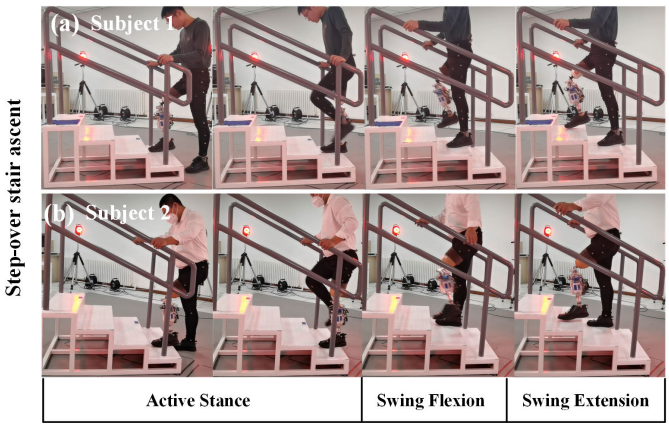

Fig. 9. The subjects wear the HSAK in step-over stair ascent.

In level walking, the angle and torque of the hip and knee joints were measured through the integrated infrared motion capture system and force plate system. In stair ascent, the systems can only obtain the angle of the hip and knee joints. Thus, the knee torque was estimated based on motor current data recorded via the embedded system. In addition, each step was 0.13m high of the stairs. Both subjects used TEHLIN 4P03 (pneumatic non-MPK) as their daily use knees. In both types of experiments, they first performed the test with their daily prostheses, and then with the HSAK prosthesis. Before the experiments, all subjects were trained with the HSAK (1) to adapt to the HSAK and the controller; (2) to allow tuning controller parameters to suit each subject; (3) to roughly match their proficiency with their PKs. All of the above experiments were approved by the Second Hospital of Jilin University (No. 2021072), and the subjects provided informed consent before the experiments.

Fig.10 to Fig.13 show a comparison of each participant's daily-use devices and the HSAK in level walking and stair ascent, respectively. As shown in every figure, the mean of the prosthetic side data is represented by a thick colored line, and the shaded range is the standard deviation of the data. The healthy data from [34] are shown in black lines for reference. As the subjects were unable to complete step-over stair ascent with the daily-use devices, we recorded two steps of the affected side information in step-by-step stair ascent. The test data showed that the average power consumption of

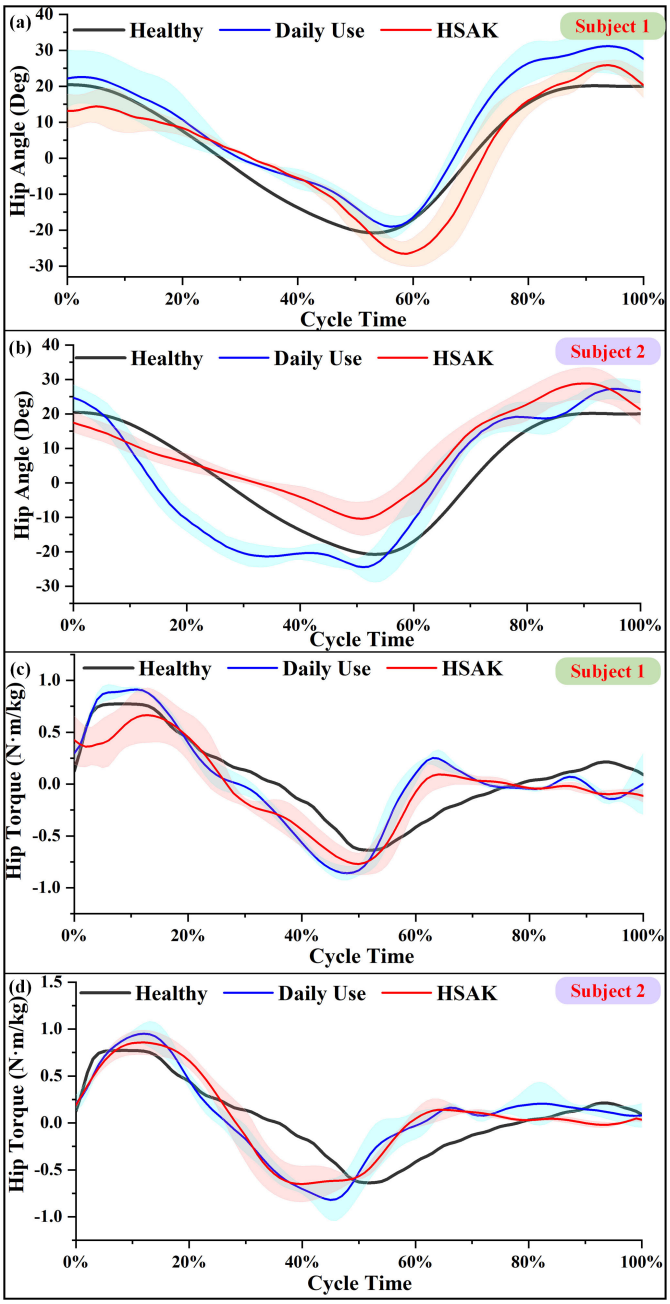

Fig. 10. Hip angle and torque for level walking.

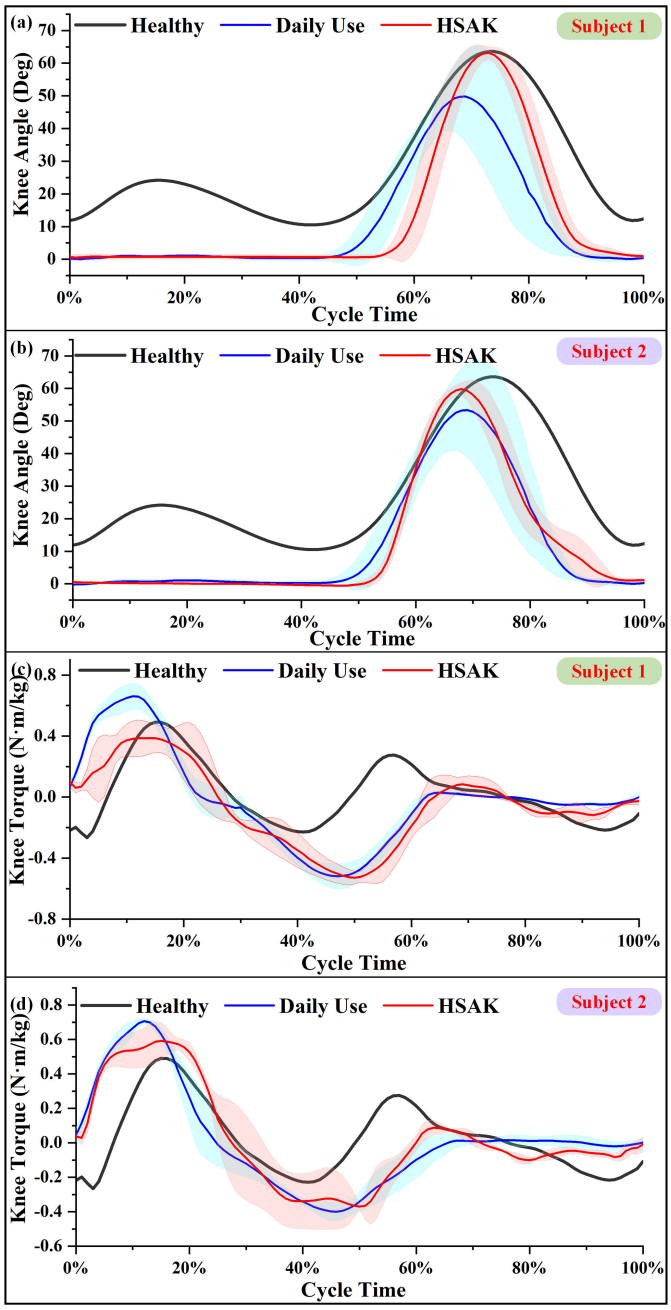

Fig. 11. Knee angle and torque for level walking.

the HSAK was 22J per gait cycle in level walking and 121J per gait cycle in step-over stair ascent. At this rate, the 2800mAh batteries would support approximately walking 11000 steps or climbing 4000 steps on stairs.

Gait symmetry is an important index of prosthesis evaluation [25]. Symmetry is calculated by two parameters: correlation coefficient (CC) and percentage range of angle change (PRA). The CC can compare the shape similarity of the two curves, but not the amplitude. Therefore, the PRA is introduced and calculated as follows.

$$PRA = \frac{RA_a - RA_h}{RA_h} \times 100\% \tag{17}$$

RA_a and RA_h represent the angle range of the affected side and the healthy side respectively. In addition, as described in the Section I, we expect to be compatible with low passive friction and high torque output through the HSAK. Therefore, the peak knee flexion angle in level walking and the peak active extension torque in stair ascent are also important evaluation indicators.

A. Level Walking

Fig.10 shows the hip joint angle and torque results for level walking. The movement angle of the hip joint when the subjects used the HSAK prosthesis (CC: 0.96, PRA: −5.26%) was closer to that of the healthy hip joint, relative to their daily use prostheses (CC: 0.94, PRA: +19.24%). Furthermore, the HSAK increased the CC value of hip torque from 0.82 to 0.84, while root mean square (RMS) value of hip torque decreased

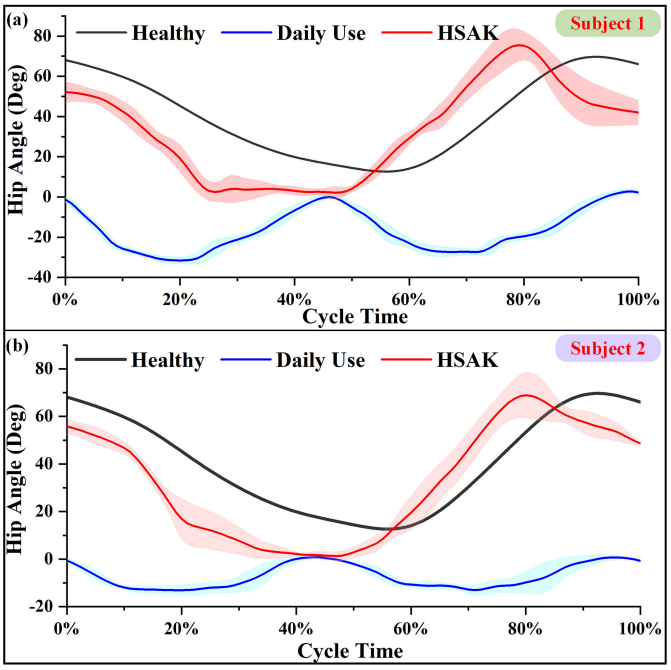

Fig. 12. Hip angle for stair ascent.

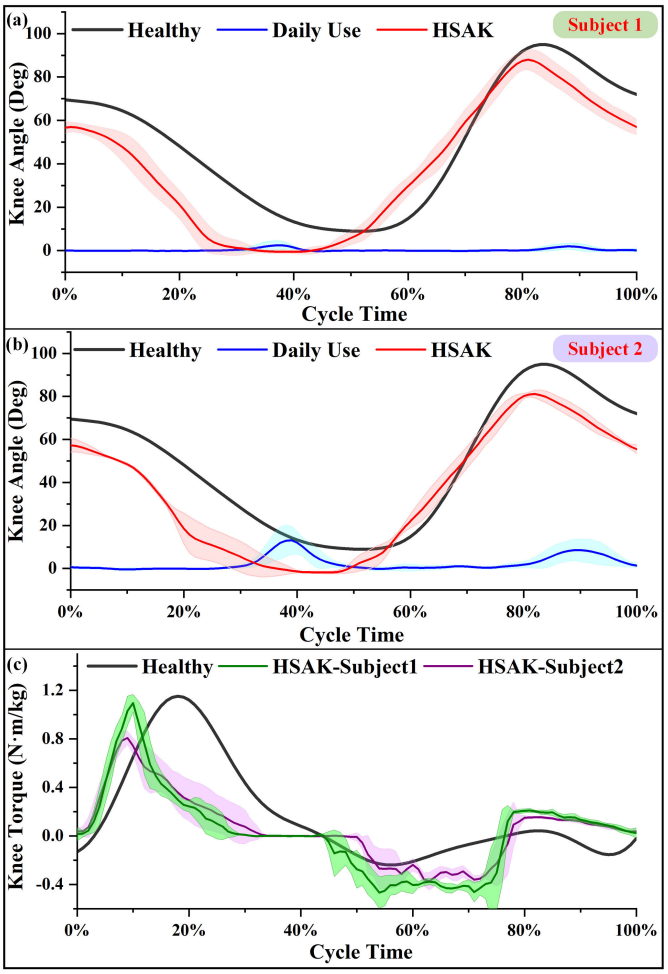

Fig. 13. Knee angle and torque for stair ascent.

from 0.45Nm/kg to 0.42Nm/kg. Additionally, as shown in Fig.11, which displays the knee angle and torque results for level walking. Compared with the daily use prosthesis, the knee trajectory using the HSAK, was more correlated with the healthy data (CC of daily use: 0.88, CC of HSAK: 0.94) and the total range is closer to the health data (PRA of daily use: −21.07%, PRA of HSAK: −9.53%). Moreover, the knee angle curves show that the HSAK supported the weight of the amputee with no knee flexion in the ES phase, which verified the locking ability of the rotary valve. Due to the low passive friction, the peak knee flexion angle in the passive SF phase produced by the subjects wearing the HSAK (59.34°) was equivalent to 93.34% of the healthy body, while that produced by daily use devices (51.57°) was equivalent to 81.12%. Meanwhile, the CC value of the knee torque corresponding to the daily use of the prosthesis was 0.56, while that to the HSAK prosthesis was 0.46.

B. Step-Over Stair Ascent

Amputees with the HSAK and healthy subjects can complete the step-over stair ascent, so a complete gait is defined as the heel striking the first stair to the heel striking the third stair. When wearing the daily use knee, the affected side cannot cross the second stair and had to climb stairs step by step to the third stair. As shown in Fig.12, when the HSAK was employed, the hip angle (CC: 0.73) was significantly closer to the healthy data compared to prostheses used daily (CC: 0.12). When wearing the HSAK, in order to ensure that the affected side smoothly crosses the stairs, the maximum flexion angle of the hip was higher than the healthy side, which further led to a larger PRA (+28.89%). When wearing daily prostheses, the hip range of motion was obviously smaller (PRA: −26.82%) because the subjects could only go ascent with step-to stair. In Fig.13, when using the daily use devices, the almost unbending knee joint resulted in quite low CC and PRA values (CC: 0.04, PRA: −84.94%). In contrast, when the HSAK was used, an obvious knee flexion and extension process was observed (average peak knee flexion of 83.39°), and the CC and PRA values (CC: 0.93, PRA: +1.09%) were significantly improved. At the beginning of the gait cycle, the initial knee angles of the HSAK (57.01°) were less than that of healthy people (68.51°). In the AS phase, the peak normalized torque generated by the HSAK for the two objects were 1.09Nm/kg and 0.81Nm/kg, respectively, which means that the maximum output torque was more than 60Nm.

V. Discussion

A. Characteristics of the HSAK and Tradeoffs Relative to Other Prosthesis Types

HSAK developed a closed hydraulic system that integrates the active drive and damping control subsystems while operated independently. For level walking, during the early stance phase the HSAK provided stable support through the locked joint via the valve while consuming no electrical energy except for the necessary hardware circuits. Subsequently, during the swing phase, the prosthesis provided free flexion via the damping subsystem and power extension via the active subsystem. For stair ascent, the active subsystem worked all the time.

The HSAK outputted sufficient torque during the active stance phase and offered adequate flexion angle to cross the stairs during the swing phase. In addition, the battery can meet the endurance needs of amputees' daily activities.

The HSAK significantly improves knee flexion angle (Fig.11 and Fig.13) and gait symmetry, relative to the conventional PKs in daily use, especially in stair ascent (Fig.12 and Fig.13). As also the hip torque required for walking was reduced by 7% by the HSAK (Fig.10). Our preliminary validation of the two amputees shows a good biomechanical match between the affected side and the healthy side. When compared to other SAKs, the HSAK eliminates the mechanical devices of gears and lead screws through the two separate subsystems and solves incompatible problems with both free swing (Fig.11) and adequate torque output (Fig.13).

In Fig.11, the HSAK flexed naturally following the stump movement in the PS and SF phases like the PKs. Despite passive motion, the maximum flexion angle was about 60° due to low friction, which satisfies the swing clearance requirement and is comparable to the active swing flexion prosthesis [22], [26]. Then, in the SE phase, the knee joint was fully extended by the active motor to strengthen the stability of walking, which like the active extension prosthesis [23]. In Fig.13, HSAK produced adequate peak torque (more than 60Nm) to help amputees climb stairs, comparable to AKs [7], [14], [22]. Thus, as a SAK, the HSAK achieves the flexibility of passive prosthesis, the stability of active prosthesis, and the powerful active torque by considering both low passive friction and large active transmission ratio.

The HSAK adds the hydraulic damping adjustment elements in comparison to AKs, and adds a hydraulic pump and a higher power motor in comparison to other semi-active prostheses. In addition, a large capacity battery of 2800mAh was selected. These components result in an increase in the weight of the prosthesis, but it is worth it compared to the advantages of the driveline.

The performance parameters of HSAK and several typical prosthesis knees are compared as shown in Table I. The Utah AVT Knee [18] is a semi-active prosthesis with a larger transmission ratio, but does not permit rapid transition between low impedance and high torque. Compared with [19], the HSAK can quickly shift motion modes. In addition, the HSAK provides variable damping in flexing and active assist in extending rather than fixed damping. Compared to other semi-active knee joints [23] and [26], the HSAK can output about 6 times of active torque.

B. Limitations

For safety reasons, the knee was locked in the ES phase of level walking, which limits further improvement of gait symmetry and the leads to increase hip work and power [35]. In some cases, the electric prosthesis recovers electrical energy during swing flexion [22], while the HSAK cannot recover and consumes a little energy to adjust the damping force. As in stair ascent, in comparison with healthy human data [34], the HSAK supplies a smaller initial knee and hip angle. Because the artificial foot with no dorsiflexion affected the knee and hip further flexion. In addition, HSAK is heavier than semi-active prostheses [23], [26], less than or close to active prostheses [12], [22], which is a limiting factor for further application.

TABLE I
COMPARISON OF PERFORMANCE PARAMETERS OF TYPICAL PROSTHETIC KNEES

	Motor Type	Nominal Power/W	Transmission Ratio	Continuous Torque/Nm	Weigh /kg	Driving Type
HSAK	**Maxon EC flat 60**	**150**	**126-174:1**[a]	**38-52**[b]	**2.68**	**SAK**
Low-Impedance Leg [22]	Robodrive ILM 85x26	410	22:1	57.2	3.0[c]	AK
UTD Leg-Knee [7]	Maxon EC 4 pole-30	200	360:1	34	3.5[c]	AK
OSL-Knee [13]	T-motor U8	400[c]	49.4:1	47	2.3	AK
Utah AVT Knee [18]	Maxon EC 4 pole-22	120	25-375:1	1-20	1.7	SAK
SACA Knee [23]	Maxon EC 22	90	75:1	7.5	2.2	SAK
RTFP Knee [26]	Faulhaber 3257G024CR	60	21:1	8	2.2	SAK

[a]Calculated based on typical knee angle range from 0° to 90°; [b]Estimated with nominal motor torque, transmission ratio and 75% overall efficiency;[c]Estimated value.

VI. CONCLUSION

This study developed a hydraulic semi-active knee (HSAK) prosthesis as a new solution for active knee prostheses. The most current active knee prostheses driven by hydraulic-mechanical coupling or electromechanical systems always lead to the incompatibilities between the low passive friction and high transmission ratio. To solve the problem, the HSAK integrates independent active and damping subsystems. The damping subsystem provides damping adjustment to meet low passive friction and high damping support, and the active subsystem provides high transmission ratio to offer adequate torque. The design, manufacture and experiments of the proposed prosthesis are presented in detail.

In bench-top experiments, the drive system provides a minimum passive motion resistance of 3N and a maximum passive auxiliary torque of 4.42Nm. In human subject experiments, the HSAK significantly improves knee flexion angle and gait symmetry compared with the daily-use devices. In level walking, due to low friction, the HSAK passively follows the thigh stump movement with a maximum flexion angle of about 60°, comparable to the active swing prostheses [22], [26]. Then the prosthesis provides active assistance to fully extend the knee joint in swing extension like an active knee. In stair ascent walking, the peak active torque generated by the HSAK is more than 60Nm, comparable to AKs [7], [13], [22]. The new design proposed a way to endow the knee prosthesis with the flexibility of the passive prostheses, the stability of the active prostheses and the powerful active torque. One limitation of the HSAK is weight and could be improved in the future with smaller pumps and actuators.

REFERENCES

[1] C. Chen, M. Hanson, R. Chaturvedi, S. Mattke, R. Hillestad, and H. H. Liu, "Economic benefits of microprocessor controlled prosthetic knees: A modeling study," *J. Neuroeng. Rehabil.*, vol. 15, no. S1, p. 62, Sep. 2018.

[2] M. P. Mileusnic, L. Rettinger, M. J. Highsmith, and A. Hahn, "Benefits of the genium microprocessor controlled prosthetic knee on ambulation, mobility, activities of daily living and quality of life: A systematic literature review," *Disab. Rehabil., Assistive Technol.*, vol. 16, no. 5, pp. 453–464, Jul. 2021.

[3] J. Perry, J. M. Burnfield, C. J. Newsam, and P. Conley, "Energy expenditure and gait characteristics of a bilateral amputee walking with C-leg prostheses compared with stubby and conventional articulating prostheses," *Arch. Phys. Med. Rehabil.*, vol. 85, no. 10, pp. 1711–1717, Oct. 2004.

[4] V. J. Harandi et al., "Gait compensatory mechanisms in unilateral transfemoral amputees," *Medical Eng. Phys.*, vol. 77, pp. 95–106, Mar. 2020.

[5] T. Gjovaag, P. Mirtaheri, and I. M. Starholm, "Carbohydrate and fat oxidation in persons with lower limb amputation during walking with different speeds," *Prosthetics Orthotics Int.*, vol. 42, no. 3, pp. 304–310, Jun. 2018.

[6] R. Fluit, E. C. Prinsen, S. Wang, and H. van der Kooij, "A comparison of control strategies in commercial and research knee prostheses," *IEEE Trans. Biomed. Eng.*, vol. 67, no. 1, pp. 277–290, Jan. 2020.

[7] D. E. Quintero, D. J. Villarreal, D. J. Lambert, S. Kapp, and R. D. Gregg, "Continuous-phase control of a powered knee–ankle prosthesis: Amputee experiments across speeds and inclines," *IEEE Trans. Robot.*, vol. 34, no. 3, pp. 686–701, Jun. 2018.

[8] S. Kumar, A. Mohammadi, D. Quintero, S. Rezazadeh, N. Gans, and R. D. Gregg, "Extremum seeking control for model-free auto-tuning of powered prosthetic legs," *IEEE Trans. Control Syst. Technol.*, vol. 28, no. 6, pp. 2120–2135, Nov. 2020.

[9] B. E. Lawson, H. A. Varol, A. Huff, E. Erdemir, and M. Goldfarb, "Control of stair ascent and descent with a powered transfemoral prosthesis," *IEEE Trans. Neural Syst. Rehabil. Eng.*, vol. 21, no. 3, pp. 466–473, May 2013.

[10] B. E. Lawson, J. Mitchell, D. Truex, A. Shultz, E. Ledoux, and M. Goldfarb, "A robotic leg prosthesis: Design, control, and implementation," *IEEE Robot. Automat. Mag.*, vol. 21, no. 4, pp. 70–81, Dec. 2014.

[11] B. E. Lawson, E. D. Ledoux, and M. Goldfarb, "A robotic lower limb prosthesis for efficient bicycling," *IEEE Trans. Robot.*, vol. 33, no. 2, pp. 432–445, Apr. 2017.

[12] T. Elery, S. Rezazadeh, C. Nesler, and R. D. Gregg, "Design and validation of a powered knee–ankle prosthesis with high-torque, low-impedance actuators," *IEEE Trans. Robot.*, vol. 36, no. 6, pp. 1649–1668, Dec. 2020.

[13] S. Bedard and P. Roy, "Actuated prosthesis for amputees," U.S. Patent 9 358 137 B2, Jun. 7, 2016.

[14] A. F. Azocar, L. M. Mooney, J. Duval, A. M. Simon, L. J. Hargrove, and E. J. Rouse, "Design and clinical implementation of an open-source bionic leg," *Nature Biomed. Eng.*, vol. 4, no. 10, pp. 941–953, Oct. 2020.

[15] M. Pi, Z. Li, Q. Li, Z. Kan, and C. Yang, "Biologically inspired deadbeat control of robotic leg prostheses," *IEEE/ASME Trans. Mechatronics*, vol. 25, no. 6, pp. 2733–2742, Dec. 2020.

[16] L. Flynn et al., "The challenges and achievements of experimental implementation of an active transfemoral prosthesis based on biological quasi-stiffness: The CYBERLEGs beta-prosthesis," *Frontiers Neurorobot.*, vol. 12, p. 80, Dec. 2018.

[17] S. Heins, L. Flynn, J. Geeroms, D. Lefeber, and R. Ronsse, "Torque control of an active elastic transfemoral prosthesis via quasi-static modelling," *Robot. Auto. Syst.*, vol. 107, pp. 100–115, Sep. 2018.

[18] E. J. Rouse, L. M. Mooney, and H. M. Herr, "Clutchable series-elastic actuator: Implications for prosthetic knee design," *Int. J. Robot. Res.*, vol. 33, no. 13, pp. 1611–1625, 2014.

[19] T. Lenzi, M. Cempini, L. Hargrove, and T. Kuiken, "Design, development, and testing of a lightweight hybrid robotic knee prosthesis," *Int. J. Robot. Res.*, vol. 37, no. 8, pp. 953–976, Jul. 2018.

[20] M. Tran, L. Gabert, M. Cempini, and T. Lenzi, "A lightweight, efficient fully powered knee prosthesis with actively variable transmission," *IEEE Robot. Autom. Lett.*, vol. 4, no. 2, pp. 1186–1193, Apr. 2019.

[21] J. Mendez, S. Hood, A. Gunnel, and T. Lenzi, "Powered knee and ankle prosthesis with indirect volitional swing control enables level-ground walking and crossing over obstacles," *Sci. Robot.*, vol. 5, no. 44, Jul. 2020.

[22] T. Elery, S. Rezazadeh, E. Reznick, L. Gray, and R. D. Gregg, "Effects of a powered knee-ankle prosthesis on amputee hip compensations: A case series," *IEEE Trans. Neural Syst. Rehabil. Eng.*, vol. 28, no. 12, pp. 2944–2954, Dec. 2020.

[23] H. L. Bartlett, B. E. Lawson, and M. Goldfarb, "Optimal transmission ratio selection for electric motor driven actuators with known output torque and motion trajectories," *J. Dyn. Syst., Meas., Control*, vol. 139, no. 10, Oct. 2017, Art. no. 101013.

[24] J. T. Lee, H. L. Bartlett, and M. Goldfarb, "Design of a semipowered stance-control swing-assist transfemoral prosthesis," *IEEE/ASME Trans. Mechatronics*, vol. 25, no. 1, pp. 175–184, Feb. 2020.

[25] J. T. Lee and M. Goldfarb, "Effect of a swing-assist knee prosthesis on stair ambulation," *IEEE Trans. Neural Syst. Rehabil. Eng.*, vol. 29, pp. 2046–2054, Oct. 2021, doi: 10.1109/TNSRE.2021.3116787.

[26] S. Gao, J. Mai, J. Zhu, and Q. Wang, "Mechanism and controller design of a transfemoral prosthesis with electrohydraulic knee and motor-driven ankle," *IEEE/ASME Trans. Mechatronics*, vol. 26, no. 5, pp. 2429–2439, Oct. 2021.

[27] T. Yu, A. R. Plummer, P. Iravani, J. Bhatti, S. Zahedi, and D. Moser, "The design, control, and testing of an integrated electrohydrostatic powered ankle prosthesis," *IEEE/ASME Trans. Mechatronics*, vol. 24, no. 3, pp. 1011–1022, Jun. 2019.

[28] X. Tian, S. Wang, X. Wang, D. Dong, and Y. Zhang, "Design and control of a compliant electro-hydrostatic-powered ankle prosthesis," *IEEE/ASME Trans. Mechatronics*, vol. 27, no. 5, pp. 2429–2439, Oct. 2022.

[29] T. Ko, H. Kaminaga, and Y. Nakamura, "Key design parameters of a few types of electro-hydrostatic actuators for humanoid robots," *Adv. Robot.*, vol. 32, no. 23, pp. 1241–1252, Dec. 2018.

[30] Q. L. Zeng, J. Cui, and W. M. Zhao, "Simulation analysis for hydraulic clamping force of bidirectional hydraulic Lock' valve spool based on fluent," *Adv. Mater. Res.*, vols. 542–543, pp. 1091–1095, Jun. 2012.

[31] M. Zhu, S. Zhao, and J. Li, "Design and analysis of a new high frequency double-servo direct drive rotary valve," *Frontiers Mech. Eng.*, vol. 11, no. 4, pp. 344–350, Dec. 2016.

[32] D. A. Winter, *Biomechanics and Motor Control of Human Movement*, 2nd ed. New York, NY, USA: Wiley, 2009.

[33] H. Wang, G. Gong, H. Zhou, and W. Wang, "Steady flow torques in a servo motor operated rotary directional control valve," *Energy Convers. Manage.*, vol. 112, pp. 1–10, Mar. 2016.

[34] R. Riener, M. Rabuffetti, and C. Frigo, "Stair ascent and descent at different inclinations," *Gait Posture*, vol. 15, no. 1, pp. 32–44, 2002.

[35] J. Geeroms, L. Flynn, R. Jimenez-Fabian, B. Vanderborght, and D. Lefeber, "Design and energetic evaluation of a prosthetic knee joint actuator with a lockable parallel spring," *Bioinspiration Biomimetics*, vol. 12, no. 2, Feb. 2017, Art. no. 026002.